JCIM JOURNAL OF CHEMICAL INFORMATION AND MODELING

pubs.acs.org/jcim Article

Selectivity and Ranking of Tight-Binding JAK-STAT Inhibitors Using Markovian Milestoning with Voronoi Tessellations

Anupam Anand Ojha, Ambuj Srivastava, Lane William Votapka, and Rommie E. Amaro*

Cite This: J. Chem. Inf. Model. 2023, 63, 2469−2482 Read Online

ACCESS | Metrics & More | Article Recommendations | Supporting Information

ABSTRACT: Janus kinases (JAK), a group of proteins in the nonreceptor tyrosine kinase (NRTKs) family, play a crucial role in growth, survival, and angiogenesis. They are activated by cytokines through the Janus kinase−signal transducer and activator of a transcription (JAK-STAT) signaling pathway. JAK-STAT signaling pathways have significant roles in the regulation of cell division, apoptosis, and immunity. Identification of the V617F mutation in the Janus homology 2 (JH2) domain of JAK2 leading to myeloproliferative disorders has stimulated great interest in the drug discovery community to develop JAK2-specific inhibitors. However, such inhibitors should be selective toward JAK2 over other JAKs and display an extended residence time. Recently, novel JAK2/STAT5 axis inhibitors (N-(1H-pyrazol-3-yl)pyrimidin-2-amino derivatives) have displayed extended residence times (hours or longer) on target and adequate selectivity excluding JAK3. To facilitate a deeper understanding of the kinase−inhibitor interactions and advance the development of such inhibitors, we utilize a multiscale Markovian milestoning with Voronoi tessellations (MMVT) approach within the Simulation-Enabled Estimation of Kinetic Rates v.2 (SEEKR2) program to rank order these inhibitors based on their kinetic properties and further explain the selectivity of JAK2 inhibitors over JAK3. Our approach investigates the kinetic and thermodynamic properties of JAK−inhibitor complexes in a user-friendly, fast, efficient, and accurate manner compared to other brute force and hybrid-enhanced sampling approaches.

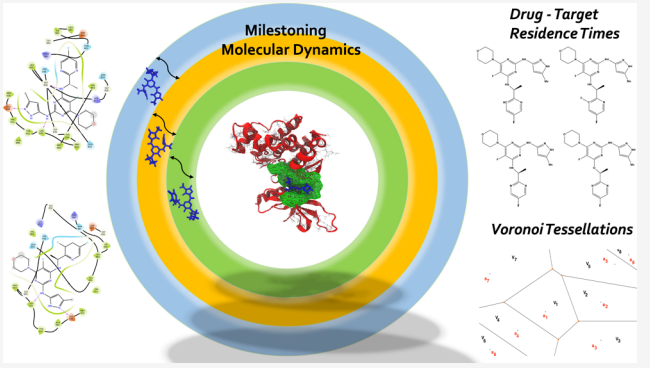

1. INTRODUCTION

Tyrosine kinases (TKs), a family of proteins, catalyze the transfer of phosphate groups from adenosine triphosphate (ATP) molecules to tyrosine residues of the target protein.[1,2] The TKs can be broadly divided into receptor and nonreceptor tyrosine kinases. The receptor tyrosine kinases (RTKs) are membrane bound and pass the extracellular signal to the inside of cells, while nonreceptor tyrosine kinases (nRTKs) are mainly cytosolic and bind to ligands to activate downstream signaling.[3−5] nRTKs are involved in cell signaling, differentiation, proliferation, and apoptosis. Janus kinase (JAK) proteins are nRTK receptors involved in activating transcription and production of cytokines to recruit immune cells at the site of infections. The JAK family comprises Janus kinase 1 (JAK1), Janus kinase 2 (JAK2), Janus kinase 3 (JAK3), and tyrosine kinase 2 (TYK2).[6,7] JAKs regulate downstream signaling by activating signal transducer and activator of transcription (STAT) proteins propagating the signal from the membrane to the nucleus, also known as the JAK-STAT pathway.[7−9] The JAK-STAT pathway regulates cytokines and growth hormones which are crucial for cellular processes, such as hematopoiesis, lactation, immune system development, and immune response.[10] The abnormalities and mutations in JAK proteins lead to neurological and immune system defects, including, but not limited to, rheumatoid arthritis (RA), inflammatory bowel diseases (IBD), multiple sclerosis (MS), and cancer.[11,12] Mutations in JAK1 and JAK3 are especially known to cause severe combined immune deficiency (SCID) diseases.[13]

The JAK proteins are constitutively expressed, with the exception of JAK3 proteins, which are expressed upon immune activation. JAK proteins contain seven conserved homology domains (JH1−JH7).[14,15] The JH1 domain at the carboxyl-terminal shows a classical tyrosine kinase activity, while the JH2 domains are pseudokinase domains that assist the JH1 domain for catalysis. JH3−JH7 domains are known to be involved in receptor binding and the regulation of kinase activity. Inhibition of JAK proteins may prove to be effective against diseases, including neurological disorders and different types of cancer. The similarity and structural conservation in

Received: December 15, 2022
Published: April 6, 2023

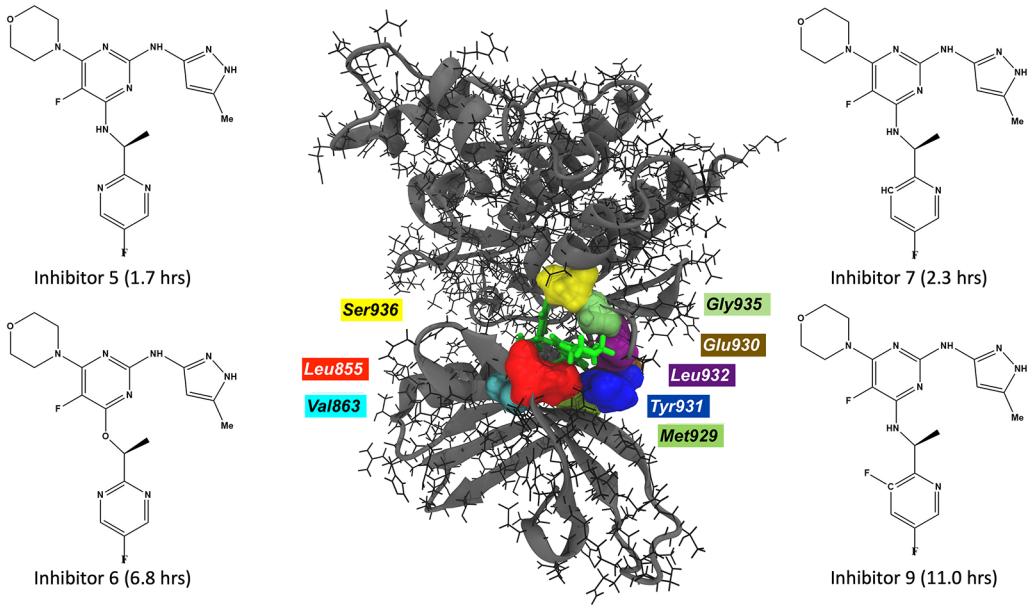

Figure 1. JAK2−inhibitor 9 complex with interacting residues within a cutoff distance of 2.5 Å (center). The inhibitors with large residence times for JAK2 proteins are displayed.

JAK proteins create challenges to designing selective inhibitors against them.[16,17] Although both the JAK2 and JAK3 proteins have highly conserved domains and are structurally very similar, one of the significant differences between them are the interactions of these proteins with different types of receptors. While JAK2 primarily mediates signals from glycoprotein 130 (gp130)-related cytokines, granulocyte macrophage-colony stimulating factor (GM-CSF) receptors, and type II cytokine receptors, JAK3 mediates signaling from type I receptors containing the common gamma chain (γc).[18−21] JAK inhibitors have shown promise as potential treatments for a variety of diseases, including certain types of cancer, autoimmune disorders, and inflammatory conditions.[22−27] Tofacitinib and baricitinib are the two first-generation drugs that the U.S. Food and Drug Administration (FDA) and the European Medicines Agency (EMA) have approved for the treatment of RA.[28−30] Tofacitinib targets JAK1, JAK2, and JAK3, while baricitinib targets JAK1 and JAK2 proteins. However, selective inhibition of JAK proteins is crucial for tuning the signaling pathway and the underlying downstream processes. Structural understanding of selective inhibition is crucial to optimize their activities and design better selective inhibitors.[31]

Molecular dynamics (MD) simulations have been effective in studying the binding and unbinding dynamics of protein−-inhibitor complexes and can be used for kinetic estimates.[32−43] Understanding the receptor−ligand binding and unbinding process can be useful for drug discovery and development, especially in accelerating lead optimization efforts and lowering drug attrition rates.[44−46] The bimolecular association rate constant (k_{on}) and the dissociation rate constant (k_{off}) are required to describe the kinetic profile of a potential noncovalent inhibitor or a drug molecule. Recently, drug−target residence time ($1/k_{off}$), or the time spent by the drug in the binding pocket of the protein, has received significant attention as drugs with a higher residence time are shown to have greater *in vivo* efficacy as compared to thermodynamic parameters such as free energy.[47−50] It is possible for drugs with similar binding free energies (ΔG_{bind}) to have different binding and unbinding kinetic rates. Several factors contribute to ligand binding and unbinding kinetics. These include, but are not limited to, the size and flexibility of ligands, forces within the molecular system, large-scale receptor conformational rearrangements, and ligand-induced conformational changes in the receptor.[51−57] One of the major limitations of MD simulations is the immense amount of computation time required to observe rare biologically relevant events. Simulations often get stuck in metastable regions. Enhanced sampling methods including and not limited to metadynamics,[58−62] adaptive biasing force (ABF),[63−65] and umbrella sampling[66,67] are employed to overcome such limitations where the applied bias potential steers the system to overcome deep energy wells. The bias potential for these methods is a function of collective variables (CVs), which are predefined and often require an in-depth understanding of the biological systems of interest.

Gaussian accelerated molecular dynamics (GaMD) is an enhanced sampling method where a harmonic boost potential is added to the total potential energy of the system, leading to reduced energy barriers.[68,69] An implementation of GaMD for receptor−ligand complexes is Ligand GaMD (LiGaMD), where a potential energy boost is applied to the ligand nonbonded interaction potential energy while another boost is applied to the remaining potential energy of the entire system, thus facilitating accelerated ligand binding and unbinding events.[70,71] Random acceleration molecular dynamics (RAMD) is another method used to rank inhibitors by residence time for a particular receptor.[40,72] Scaled MD is an unbiased sampling approach that can be used to predict protein−ligand unbinding kinetics.[36] Other methods, including free energy perturbation, can be used to obtain thermodynamic, but not kinetic, predictions for receptor−ligand binding.[73−76] A number of enhanced sampling methods exist to predict the kinetics and thermodynamics of binding and unbinding and have been summarized in recent literature.[43,77−82] A study using MM-GBSA was recently performed on a similar kinase for inhibitors bound to the ATP binding site.[83] In contrast to biasing potential methods, for the JAK systems examined in this study, Simulation-Enabled Estimation

https://doi.org/10.1021/acs.jcim.2c01589
J. Chem. Inf. Model. 2023, 63, 2469−2482

of Kinetic Rates v.2 (SEEKR2) employs a reasonably simple and uniform CV definition for receptor−ligand complexes and requires a minimal *a priori* understanding of these complexes.

N-(1H-Pyrazol-3-yl)pyrimidin-2-amino derivatives are analogous to ATP molecules and have been shown to selectively inhibit JAK2 proteins with a high residence time in the binding pocket of JAK2 as compared to JAK3 proteins (Figure 1).[84] We, therefore, aim to rank these inhibitors in comparison to their experimentally reported residence times in the JAK complexes by employing a milestoning simulation method and explain the differences in residence times by providing complete kinetic and thermodynamic profiles of receptor−ligand pairs. The SEEKR2 software is user friendly, fast, efficient, and accurate as compared to other brute force methods and hybrid approaches.[68,70,85−90] The Markovian milestoning with Voronoi tesselation (MMVT) method implemented in the SEEKR2 program is described in the Methods section followed by a detailed description of the calculation of residence times and kinetic and thermodynamic profiles of the protein−inhibitor complexes.

2. METHODS

2.1. Simulation-Enabled Estimation of Kinetic Rates v.2 (SEEKR2). *2.1.1. Markovian Milestoning with Voronoi Tessellations.* A Voronoi tessellation is a subdivision of space into n regions or "Voronoi cells".[91,92] From a given set of points $\mathbf{a} = \{a_1, a_2, a_3, \cdots, a_n\}$ and a set of Voronoi cells $\mathbf{V} = \{V_1, V_2, V_3, \cdots, V_n\}$, such that $a_1 \in V_1$, $a_2 \in V_2$, $a_3 \in V_3$, $\cdots$, $a_n \in V_n$ (Figure 2), let us define a distance metric, $d(a, b)$, that

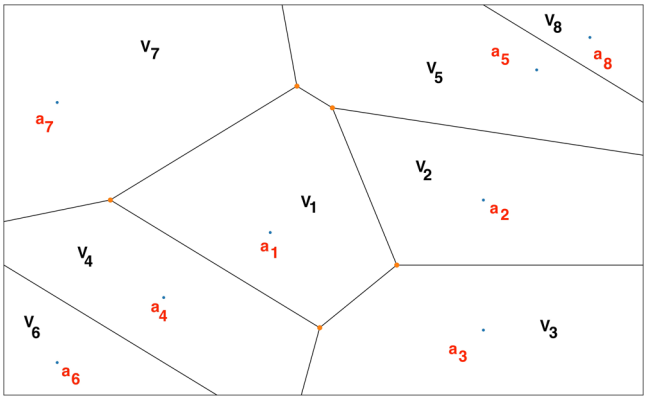

Figure 2. A representative Voronoi diagram where V_1, V_2, V_3, $\cdots$, V_n represent the Voronoi cells, and $a_1 \in V_1$, $a_2 \in V_2$, $a_3 \in V_3$, $\cdots$, $a_n \in V_n$.

estimates the distance between the two points, a and b. According to the definition of a Voronoi tessellation, a point α will belong to cell V_1 if and only if $d(a_1, \alpha) < d(a_i, \alpha)$ for $i \in \{2, 3, \cdots, n\}$. Let there be N boundaries (milestones) between adjacent Voronoi cells.

SEEKR2 is an open-source software that automates the process of preparation, initiation, running, and analysis of milestoning calculations utilizing MD and Brownian dynamics (BD) simulations to estimate the kinetics and thermodynamics of receptor−ligand binding and unbinding.[93−95] MD simulations are run using the OpenMM simulation engine, while BD simulations are run using the Browndye software.[96] In the SEEKR2 multiscale milestoning approach, the phase space of the receptor−ligand complex is split into two regions, i.e., the MD and the BD region. This partition is based on a predefined CV, i.e., the distance between the center of mass (COM) of the ligand and the COM of the receptor's binding site. In the region closer to the binding site, solvent effects and molecular flexibility must be included for describing molecular interactions; therefore, MD simulations are employed. The MD region is further partitioned into several Voronoi cells. Steered molecular dynamics (SMD) simulations are run to generate starting structures for SEEKR2 simulations.[97] SMD simulations pull the ligand slowly out of the binding pocket with a moving harmonic restraint, and a snapshot of the trajectory is saved for every Voronoi cell as it passes through them. Fully atomistic, flexible, and parallel MD simulations are performed in each Voronoi cell with reflective boundary conditions. When the ligand is further away from the binding site, i.e., in the BD region, rigid body BD simulations are adequate to describe the diffusional encounter of the ligand and the receptor.

The MMVT-SEEKR2 approach has been shown to estimate binding and unbinding kinetic and thermodynamic properties for less complex receptor−ligand systems with high accuracy, especially the model host−guest systems, i.e., β-cyclodextrin with guest ligands and the model protein system, i.e., the trypsin−benzamidine complex.[95] We thereby extend our efforts in exploring the capabilities of SEEKR2 in estimating kinetic and thermodynamic properties for more complex systems, specifically ligands which are strong binders and have large residence times.

2.1.2. Estimating Residence Times and Binding Free Energies. According to the MMVT approach, the system evolves according to a continuous-time Markov jump between Voronoi cells.[98,99] Let the rate matrix associated with the evolution be $\mathbf{Q}$, N_{ij} be the number of transitions between milestones, i and j, and R_i be the time spent by the trajectory having last touched milestone i. The diagonal and the off-diagonal elements of the transition matrix, $\mathbf{Q}$, are represented by eqs 1 and 2, respectively.

$$q_{ii} = -\sum_{j \neq i} q_{ij} \tag{1}$$

$$q_{ij} = \begin{cases} \dfrac{N_{ij}}{R_i} & \text{if } R_i \neq 0 \\ 0 & \text{if } R_i = 0 \end{cases} \tag{2}$$

MD simulations are run within the Voronoi cells until convergence is reached. Reflective boundary conditions are employed at the boundaries to confine trajectories within the Voronoi cells. Consequently, velocities of the trajectories are reversed as they touch the edges of the adjacent Voronoi cells. For a Voronoi cell α, let N_{ij}^{α} be the number of trajectory collisions with an jth milestone after having last touched the ith milestone within anchor α, let R_i^{α} be the simulation time having last touched the ith milestone within anchor α, let T_α be the total simulation time in cell α, let $N_{\alpha,\beta}$ be the total number of collisions within Voronoi cell α, with the boundary shared with Voronoi cell β, and let T be the reciprocal sum of time spent in all the cells as described by eq 3, then N_{ij} and R_i are represented by eqs 4 and 5, respectively. The equilibrium probability, π, is obtained by solving eqs 6 and 7.

$$T = \left(\sum_{\alpha=1}^{n} \frac{\pi_\alpha}{T_\alpha} \right)^{-1} \tag{3}$$

https://doi.org/10.1021/acs.jcim.2c01589
J. Chem. Inf. Model. 2023, 63, 2469−2482

$$N_{ij} = T\sum_{\alpha=1}^{n} \pi_\alpha \frac{N_{ij}^{\alpha}}{T_\alpha} \tag{4}$$

$$R_i = T\sum_{\alpha=1}^{n} \pi_\alpha \frac{R_i^{\alpha}}{T_\alpha} \tag{5}$$

$$\sum_{\beta=1,\beta\neq\alpha}^{n} \pi_\beta \frac{N_{\beta,\alpha}}{T_\beta} = \sum_{\beta=1,\beta\neq\alpha}^{n} \pi_\alpha \frac{N_{\alpha,\beta}}{T_\alpha} \tag{6}$$

$$\sum_{\alpha=1}^{n} \pi_\alpha = 1 \tag{7}$$

With $\hat{\mathbf{Q}}$ as the $N-1$ by $N-1$ matrix obtained from the upper left corner of $\mathbf{Q}$, one can compute the mean first passage time (MFPT) or residence time for each milestone described by vector $\mathbf{T}^N$ by solving eq 8.

$$\hat{\mathbf{Q}}\mathbf{T}^N = -\mathbf{1} \tag{8}$$

where $\mathbf{1}$ is a vector of ones. Stationary probabilities obtained from the milestoning simulations are used to construct the free energy profile of unbinding of the receptor−inhibitor complexes with the bound-state milestone as a reference. Stationary probabilities, $\mathbf{p}$, are found by solving the eigenvalue eq 9.

$$\mathbf{Q}\mathbf{p} = \mathbf{p} \tag{9}$$

Let k_B be Boltzmann's constant, T be the temperature, p_i be the stationary probability of the ith milestone, and p_{ref} be the stationary probability of the bound state or the reference milestone. The expression for estimating the free energy profile of the ith milestone, i.e., ΔG_i, is given by eq 10.

$$\Delta G_i = -k_B T \ln\left(\frac{p_i}{p_{ref}}\right) \tag{10}$$

2.1.3. Ranking JAK−Inhibitor Complexes with SEEKR2. N-(1H-Pyrazol-3-yl)pyrimidin-2-amino derivatives are ATP-competitive inhibitors of the JAK2-STAT5 pathway that are reported to display prolonged residence times on JAK2 and sufficient selectivity against JAK3, both at biochemical and cellular levels.[84,100] The residence times of four inhibitors with the JAK2 and JAK3 kinase were experimentally determined using a rapid dilution enzymatic assay.[101] We present a relatively computationally inexpensive and efficient application of the SEEKR2 program to predict and rank order the residence times of the JAK2 and JAK3 inhibitors.

System Preparation. To estimate the residence times of the four inhibitors in the two JAK proteins, an all-atomistic MD simulation is performed in SEEKR2. The X-ray crystal structure of the JAK2−JH1 domain in complex with inhibitor 6 (PDB ID: 3ZMM) is used as the reference structure for JAK2 SEEKR2 simulations.[84] For the preparation of the JAK2 complex with inhibitors 5, 7, and 9 (Figure 1), the X-ray crystal structure of the JAK2 domain in complex with inhibitor 6 (PDB ID: 3ZMM) is used as a reference structure. Inhibitor 6 is modified to 5, 7, and 9 using the Maestro module of the Schrödinger software suite (Figure 1).[102] Once inhibitor 6 is modified to either inhibitor 5, 7, or 9, the JAK−inhibitor complex is subjected to the removal of water molecules beyond 3 Å of the protein and with fewer than three hydrogen bonds to the neighboring residues. It is followed by hydrogen bond optimization of the receptor−ligand complex with protonation states of residues at pH 7.4. Finally, a restrained minimization of the complex is performed with a complete relaxation of the H-bond network while keeping the heavy atoms restrained. The AMBER ff14SB force field is used to parametrize the protein, while the inhibitor is parametrized using the Antechamber module with the general Amber force field (GAFF) with the AM1-BCC charge model.[103−106] The protein−inhibitor complex is then explicitly solvated with the TIP4P-Ew water model and a salt (Na+/Cl−) concentration of 150 mM in a truncated octahedral periodic box with a 10 Å water buffer.[107] The OpenMM MD engine is used to run the simulation at 300 K with a 2 fs time step and a nonbonded cutoff radius of 9 Å.[108,109] The system is systematically heated from 0 to 300 K in steps of 3 K of 20 ps each, followed by 20 ns each of NPT and NVT equilibration simulations.

The X-ray crystal structure of the JAK3−JH1 domain in complex with an indazole substituted pyrrolopyrazine (PDB ID: 3ZC6) is used as the reference structure for the JAK3 SEEKR2 simulations.[110] The inhibitor complexed with JAK3 is removed, and the structure is aligned to the JAK2 complexed with inhibitor 6. Inhibitor 6 is then placed at the ATP binding site of the JAK3 protein. Inhibitor 6 is modified to 5, 7, and 9 using the Maestro module of the Schrödinger software suite, and the same protocol is followed for JAK3 systems as performed for the JAK2 complexes for system preparation, solvation, and equilibration. It is important to note that only one crystal structure of JAK2 is used to prepare all four JAK2−inhibitor complexes, and the same holds true for the JAK3−inhibitor complexes.

Steered Molecular Dynamics and Voronoi Cell Definition. To define Voronoi cells, we described the CV as the distance between the COM of the inhibitor and the COM of α-carbons of the binding site[111] (Table S1). The cutoff distance for the binding site of the inhibitor is defined as all residues within 3 Å of any atoms of the inhibitor in its original position. All the α-carbon atoms of the surrounding residues of the JAK protein within the cutoff distance of any of the atoms of the inhibitor are defined as the binding site for the receptor−inhibitor complex. Table S1 displays the residues of each JAK−inhibitor complex selected for the COM calculation of the binding site. For JAK2−inhibitor complexes, CV-based milestones are defined as concentric spheres and are located at distances of 2.5, 3.0, 3.5, 4.0, 4.5, 5.0, 5.5, 6.0, 6.5, 7.0, 7.5, 8.0, 8.5, 9.0, 9.5, 10.0, 11.0, 12.0, 13.0, 14.0, 15.0, and 16.0 Å, respectively, from the COM of the binding site. Similarly, for the JAK3−inhibitor complexes, CV-based milestones are defined as concentric spheres and are located at distances of 3.0, 3.5, 4.0, 4.5, 5.0, 5.5, 6.0, 6.5, 7.0, 7.5, 8.0, 8.5, 9.0, 9.5, 10.0, 11.0, 12.0, 13.0, 14.0, 15.0, and 16.0 Å, respectively, from the COM of the binding site. In the case of JAK3−inhibitor complexes, none of the residues of the JAK3 protein interacted with the inhibitor within the 2.5 Å radius, leading to the choice of the first milestone at 3.0 Å. This choice should not be problematic since the milestoning procedure would not be significantly sensitive to the choice of the number of milestones as long as each state and pathway are adequately represented in each milestoning model, and the results are sufficiently converged. SMD simulations are employed to generate starting structures within each Voronoi cell where the ligand bound to the complex is slowly pulled out of the binding site in such a way that there is no significant stress to the system, and it stays in the local equilibrium. To generate starting structures for

https://doi.org/10.1021/acs.jcim.2c01589
J. Chem. Inf. Model. 2023, 63, 2469−2482

MMVT simulations, the ligand is slowly pulled from the bound state to the outermost Voronoi cell with a moving harmonic restraint of 50,000 kJ mol^{-1} nm^{-2} over the course of 1 μs.

SEEKR2 Molecular Dynamics Simulations. With the starting structures of each Voronoi cell obtained by SMD, MMVT simulations are employed with the same force field parameter files used during equilibration simulations. No harmonic restraint is applied during these simulations. Reflective boundary conditions are employed to retain the trajectories within individual Voronoi cells. A total of 400 ns of MD simulations is run within each Voronoi cell. To improve the sampling and account for stochasticity, three replicas of SEEKR2 simulations are run for each JAK−inhibitor complex. In short, three replicas of 21 independent and parallel MD simulations of 400 ns are run for each of the JAK2−inhibitor complexes, totaling a simulation time of 25.2 μs. Similarly, three replicas of 20 independent and parallel MD simulations of 400 ns within each Voronoi cell are run for each of the JAK3−inhibitor complexes, totaling a simulation time of 24 μs. For the JAK2−inhibitor and JAK3−inhibitor complexes, 21 and 20 parallel simulations, respectively, for 400 ns each were carried out on one NVIDIA V100 GPU on the Popeye computing cluster at San Diego Supercomputer Center (SDSC), which aggregated approximately 220 ns/day; i.e., the entire SEEKR2 simulations for each complex required approximately 44 h of computing time on parallel GPUs (21 and 20 parallel GPUs for JAK2−inhibitor and JAK3−inhibitor complexes, respectively). Therefore, SEEKR2 is a powerful tool for rank-ordering the ligands and characterizing the ligand binding and unbinding kinetics and thermodynamics in receptor−ligand complexes in a user-friendly and computationally efficient manner, thus facilitating computer-aided drug design.

3. RESULTS AND DISCUSSION

Estimating thermodynamic and kinetic parameters, such as the residence time and free energy of binding and unbinding, is challenging in cases of receptor−inhibitor complexes with extended residence times.[112,113] A minor change in the structures of inhibitors sometimes leads to an enormous change in the residence times in the binding pockets of proteins. We estimated the residence times of four inhibitors in the binding pocket of JAK2 and JAK3 proteins. We showed that the trend of the residence time predicted by the SEEKR2 milestoning approach captures that of experimental methods. We showed that the trend of the residence time predicted by the SEEKR2 milestoning approach reproduces the experimental findings. Inhibitors 5 and 9 displayed the lowest and the highest residence times for the JAK2 protein, respectively. Similarly, inhibitors 6 and 9 displayed the lowest and the highest residence times for the JAK3 protein, respectively (Table S2). Long time scale MD simulations are performed to study the structural aspects of protein−ligand interactions, primarily focusing on these particular inhibitors to explain the discrepancy in their respective residence times.

3.1. Determination of Kinetic and Thermodynamic Parameters from SEEKR2 Simulations. Simulations in the majority of the Voronoi cells converged after 400 ns. The MFPT or residence time is calculated using eq 8. The residence times reported in Figure 3a and b are the means of the residence times obtained from three independent SEEKR2 simulations for each of the JAK−inhibitor complexes (Table S2). Residence times for the novel series of inhibitors for JAK2 and JAK3 estimated by the SEEKR2 program are in close agreement with the experimental studies (Figure 3a and b). SEEKR2 not only predicted the residence times correctly but also preserved the rank ordering of residence times for inhibitors in both the JAK2 and JAK3 complexes. It can be seen from Figure 3a and b that inhibitors 6 and 9 display extended residence times in the ATP-binding sites of the JAK2 complexes.

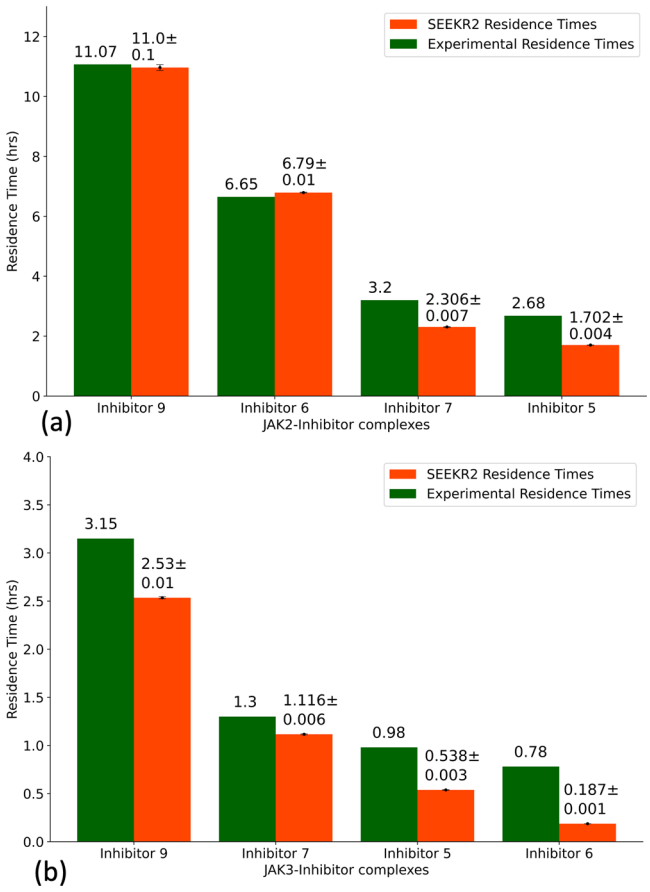

Figure 3. Residence times of JAK2 and JAK3 inhibitors as obtained from the experiments and the SEEKR2 milestoning method. The values of the residence times and the error bars for each JAK−inhibitor complex is the average of the three independent SEEKR2 calculations. (a) Residence times of the inhibitors for the JAK2 protein and (b) residence times of the inhibitors for the JAK3 protein are displayed. Error bars are present for the SEEKR2 residence time data, but they are sometimes too small be visible. An unpaired *t* test is carried out to measure the statistical significance of the difference between the experimentally determined residence times of JAK2 and JAK3 inhibitors and the SEEKR2-calculated residence times. The *p*-values obtained from the *t* test determined that there is no significant difference between the mean of the SEEKR2-calculated residence times and the experimentally determined residence times (Table S3).

ΔG_i is calculated for each of the milestones using eq 10. In the case of the JAK2−inhibitor 5 complex, two energy barriers exist as the inhibitor dissociates with the receptor, one at milestone 4 and the other at milestone 11 (Figure 4a). The COM-COM distance between the inhibitor and the alpha-carbon (α-C) atoms of the binding site for the first transition state (TS 1) is 4.50 Å, while the second transition state (TS 2) is at a COM-COM distance of 8.00 Å from the binding site. Similarly, two energy barriers exist for the JAK2−inhibitor 9 complex, one at milestone 5 and the other at milestone 13

https://doi.org/10.1021/acs.jcim.2c01589
J. Chem. Inf. Model. 2023, 63, 2469−2482

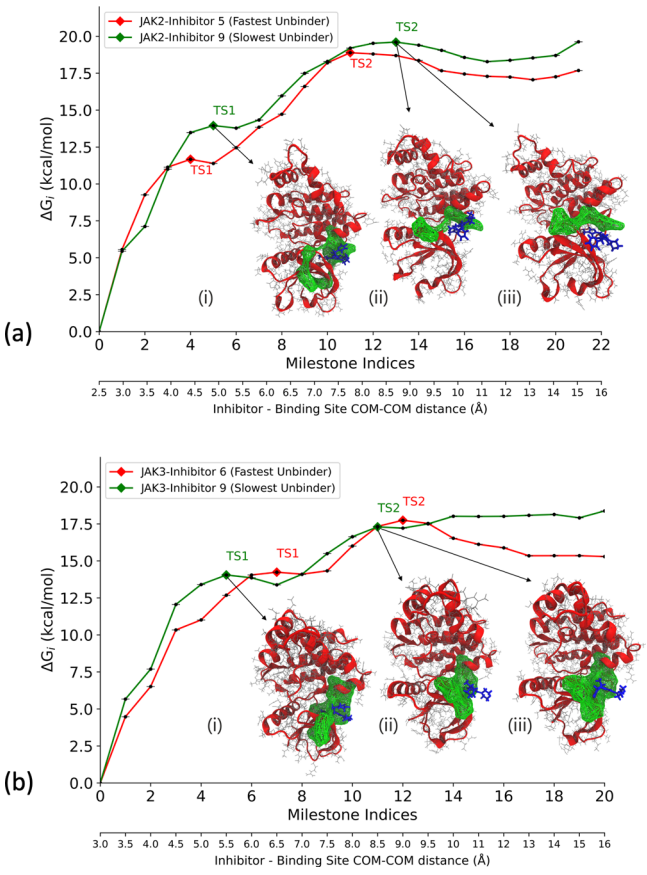

Figure 4. Free energy profile (ΔG_i) obtained from the SEEKR2 milestoning method for the JAK proteins complexed with the inhibitors. Also shown are the dominant poses of inhibitor 9 as it unbinds from the ATP binding site of JAK complexes. These poses are obtained from the SEEKR2 trajectories for milestones with the local maximum values of ΔG_i. ΔG_i values obtained for each JAK−inhibitor complex is the average of the three independent SEEKR2 calculations. The additional *X*-axis at the bottom of the graph denotes the distance between the center of masses of the inhibitor and the α carbon atoms of the binding site for each milestone. (a) ΔG_i values for the JAK2 protein complexed with inhibitor 5 and inhibitor 9 along with (i) JAK2−inhibitor 9 complex at TS 1, (ii) JAK2−inhibitor 9 complex at TS 2 (pose 1), and (iii) JAK2−inhibitor 9 complex at TS 2 (pose 2). (b) ΔG_i values for the JAK3 protein complexed with inhibitor 6 and inhibitor 9 along with (i) JAK3−inhibitor 9 complex at TS 1, (ii) JAK3−inhibitor 9 complex at TS 2 (pose 1), and (iii) JAK3−inhibitor 9 complex at TS 2 (pose 2).

(Figure 4a). TS 1 is at a COM-COM distance of 5.00 Å, while TS 2 is at a COM-COM distance of 9.00 Å from the binding site. The energy barriers for inhibitor 9 for both transitions are higher than that of inhibitor 5, indicating that inhibitor 9 is a stronger binder with a higher residence time. For the JAK3−inhibitor 6 complex, two energy barriers exist as the inhibitor dissociates with the receptor, one at milestone 7 and the other at milestone 12 (Figure 4b). The COM-COM distance between the inhibitor and the α-C atoms of the binding site for TS 1 is 6.50 Å, while TS 2 is at a COM-COM distance of 9.00 Å. Similarly, two energy barriers exist for the JAK3−inhibitor 9 complex, one at milestone 5 and the other at milestone 11 (Figure 4b). TS 1 is at a COM-COM distance of 5.00 Å, while TS 2 is at a COM-COM distance of 8.50 Å from the binding site. The energy barrier for inhibitor 9 for TS 1 is higher than that of inhibitor 6, indicating that inhibitor 9 is a stronger binder with a higher residence time.

With SEEKR2 simulations, we hold the advantage of predicting a possible ligand unbinding pathway since this methodology enables the receptor−ligand complex to undergo parallel simulations with the ligand at increasing distances from the binding site. MD trajectories within the milestones located at these transition barriers are analyzed to identify important ligand−residue interactions. For the JAK2−inhibitor 9 and JAK3−inhibitor 9 complexes, hydrogen bond (H-bond) analysis is conducted for the two identified transition states using the CPPTRAJ module of the Amber 22 package.[114−116] In the case of the JAK2−inhibitor 9 complex, for TS 1, Gly935, Tyr931, and Asp939 interacted significantly with inhibitor 9 as H-bond acceptors, while Ser936, Leu932, and Tyr931 residues were H-bond donors to inhibitor 9 (Figures 5a and 6a). On the contrary, for TS 2, interactions between the residues and inhibitor 9 decreased significantly, where the residues closer to the terminals interacted as the inhibitor gradually unbinds from the binding site (Figures 5b and 6b). In the case of the JAK3−inhibitor 9 complex, for TS 1, Tyr904 and Leu905 interacted with inhibitor 9 as H-bond acceptors and donors simultaneously (Figure 5c). For TS 2, interactions between the residues and inhibitor 9 were still significant, including Leu828 and Gly908 as major donor residues (Figure 5d). Interestingly, more residues were involved in the H-bond interactions at TS 1 for the JAK2−inhibitor 9 complex compared to the JAK3−inhibitor 9 complex. This observation can be attributed to the selectivity of inhibitor 9 toward the JAK2 protein.

SEEKR2 is able to provide kinetic and thermodynamic estimates of receptor−ligand binding and unbinding, such as residence time and free energy of binding. Selectivity of inhibitors toward JAK2/JAK3 is a complex and multifaceted concept that cannot be reduced to a single physical quantity like residence time or free energy. Instead, it encapsulates the desirable outcome that the inhibitor more preferentially binds one potential target over another, which is influenced by numerous factors, including structural differences, conformational changes, off-target effects, cellular context, and pharmacokinetics.[117−120] In this study, we focus on kinetic selectivity showing that SEEKR2 can discern a significant difference in residence times for the same set of inhibitors in JAK2 and JAK3. Recent literature studies show that thermodynamic and kinetic selectivities play the most important roles for targets of differing vulnerability, i.e., targets that require certain amounts of engagement with an inhibitor for the desired effect to be observed.[120−122] Whether a target is high or low vulnerability depends, of course, on the desired effect. The actual mechanism of that selectivity is beyond the scope of the current study. Unfortunately, SEEKR2 alone is not able to discern the selectivity mechanisms, and additional analyses must be performed, as were performed in this study with the principal component analysis (PCA) and quantum mechanical calculations.

3.2. Long Time Scale Molecular Dynamics Simulations. To understand and analyze critical aspects of binding and unbinding of the inhibitors at the ATP binding sites of JAK2 and JAK3 and to explain the discrepancy in the residence times of inhibitors and selectivity toward JAK2 over JAK3, three independent 2 μs MD simulations are run for each JAK−inhibitor complex. The starting structures in the first Voronoi cell for each receptor−inhibitor complex served as the starting structures for the long time scale MD simulations. We used the

https://doi.org/10.1021/acs.jcim.2c01589
J. Chem. Inf. Model. 2023, 63, 2469−2482

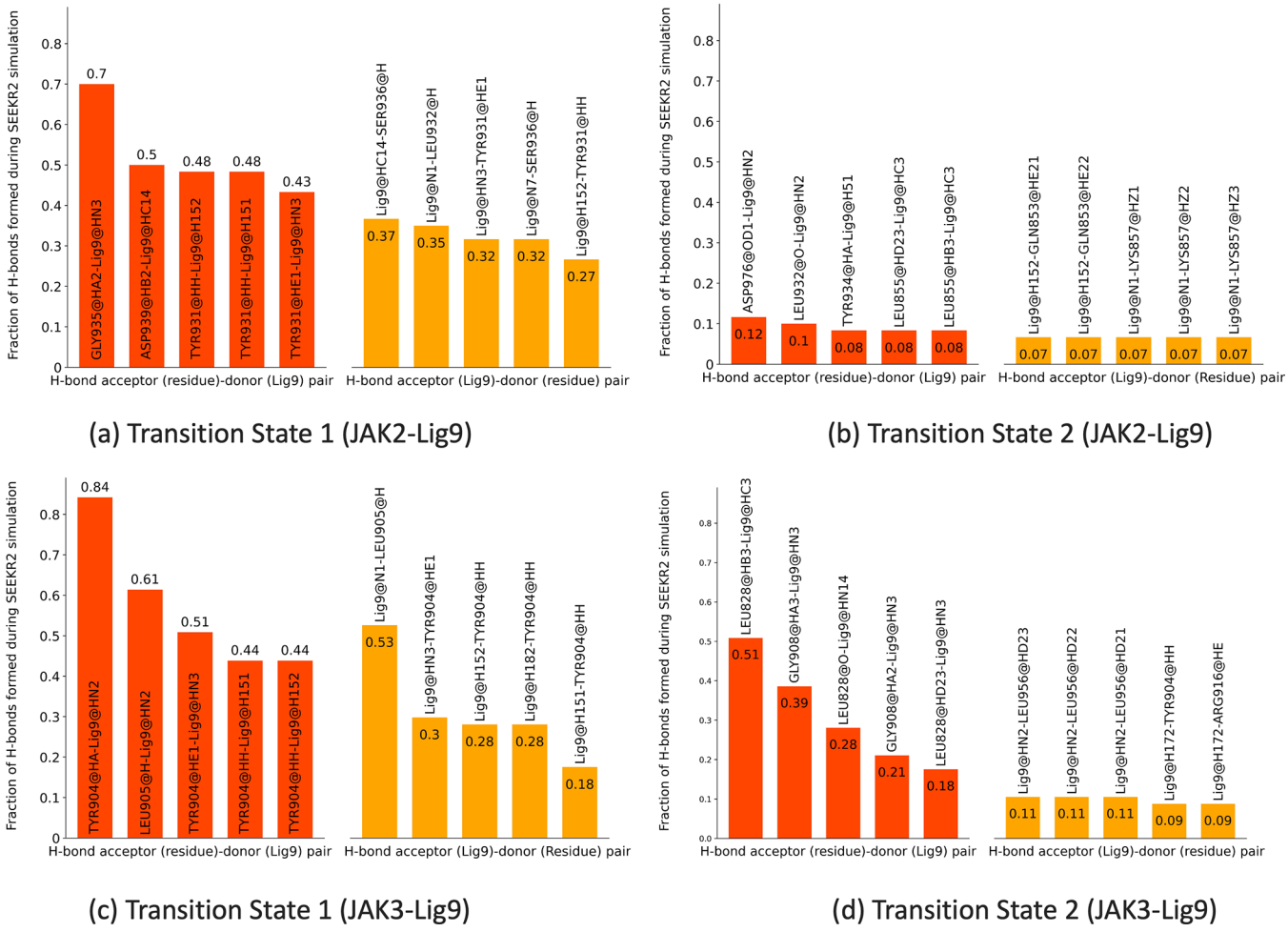

Figure 5. (a, b) Major hydrogen bond interactions formed during SEEKR2 simulations at transition states for the JAK2−inhibitor 9 complex displaying (a) TS 1 H-bond donor−acceptor pairs and (b) TS 2 H-bond donor−acceptor pairs. (c, d) Major hydrogen bond interactions formed during SEEKR2 simulations at transition states for the JAK3−inhibitor 9 complex displaying (c) TS 1 H-bond donor−acceptor pairs and (d) TS 2 H-bond donor−acceptor pairs.

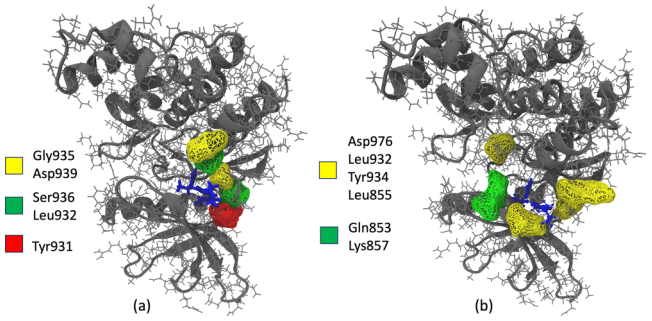

Figure 6. Major hydrogen bond interactions formed during SEEKR2 simulations for the JAK2−inhibitor 9 complex at (a) TS 1 displaying H-bond acceptor residues (yellow), H-bond donor residues (green), and H-bond donor/acceptor residues (red) and (b) TS 2 displaying H-bond acceptor residues (yellow) and H-bond donor residues (green).

same force field parameter files for the complexes as used in the SEEKR2 simulations. For each of the receptor−inhibitor complexes, a total of 6 μs of MD simulations are run at 300 K with a 2 fs time step and a nonbonded cutoff radius of 9 Å using the OpenMM MD engine. Simulation trajectories are analyzed using the CPPTRAJ module of the Amber 22 package.[114−116] Analyses including and not limited to ligand-binding site distance analysis, minimum average distance analysis, principal component analysis (PCA), and root mean squared fluctuation (RMSF) analysis are performed to gain a deeper understanding of the binding behavior of these inhibitors.

3.2.1. Discrepancy in Residence Times: Structure of Inhibitors and Their Interactions with JAKs. The inhibitors, namely 5, 6, 7, and 9, constitute a pyrazol-3-yl amine ring, a heteroaryl C-ring, and a morpholine ring (Figure 7a). Different inhibitors are synthesized by substitutions at the heteroaryl C-ring. The pyrazol-3-yl amine ring forms multiple hydrogen bonds with the ATP binding pocket of the JAKs (Figure 8a and b), and these contacts are consistent with all the inhibitors. The solvent-exposed morpholine ring does not interact much with the residues in the binding region. Interestingly, a single substitution at the heteroaryl C-ring of the inhibitor leads to a significant difference in their residence times (Figure 8c). In the case of inhibitor 9 with respect to inhibitor 5, one of the nitrogen atoms in the heteroaryl C-ring is substituted by a −CF group (Figure 8c), leading to a 5-fold increase in the residence time of inhibitor 9.

Inhibitor 9 displayed the highest residence time in both the JAK2 and JAK3 proteins. To investigate further the

https://doi.org/10.1021/acs.jcim.2c01589
J. Chem. Inf. Model. 2023, 63, 2469−2482

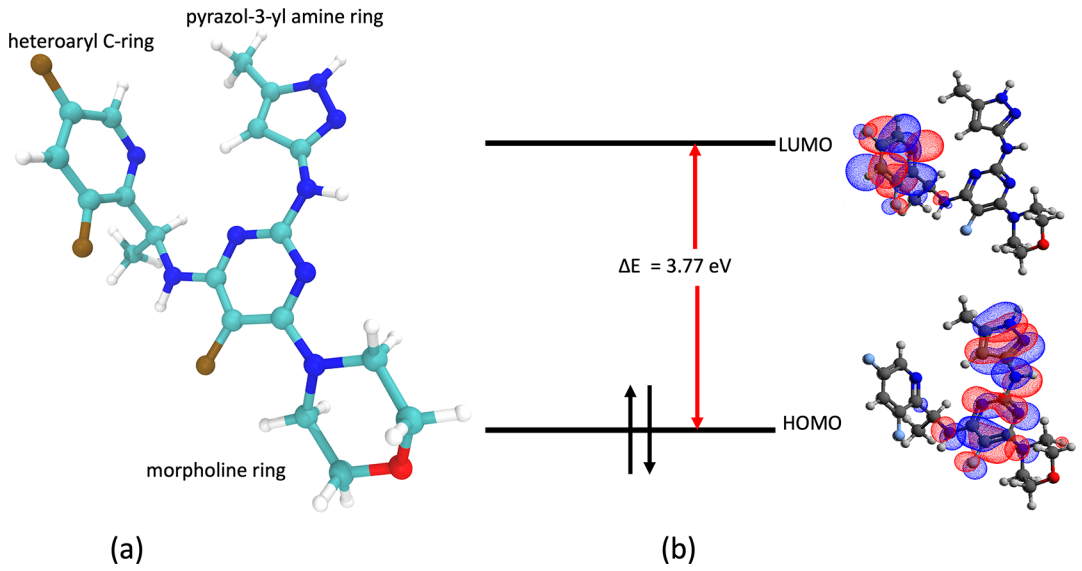

Figure 7. (a) Composition of inhibitor 9 and (b) molecular orbitals of inhibitor 9.

contributions of the heteroaryl C-ring toward the increased residence time and determine the donor−acceptor capabilities of the inhibitor, quantum mechanical (QM) calculations are run for inhibitor 5 and inhibitor 9 to determine the highest occupied molecular orbitals (HOMO) and lowest unoccupied molecular orbitals (LUMO). The Gaussian 16 suite of programs is used to carry out geometry optimization using Becke's three-parameter functional in combination with the Lee−Yang−Parr correlation functional (B3LYP) and 6-31G-(d,p) basis set.[123−126] It is observed that the heteroaryl C-ring constitutes the LUMO (Figure 7b) for all the inhibitors. The presence of an extra fluorine atom in inhibitor 9 causes extra stabilization of the bound state since the substituted fluorine atom in the heteroaryl C-ring interacts with the hydrogen of the β-carbon of the serine residue (Ser936), maintaining an average distance of 2.64 Å with a minimum distance of 2 Å (Figure 8b). In contrast, for inhibitor 5, this interaction is missing (Figure 8a). Further evidence is provided by the HOMO−LUMO energy calculations obtained from the QM calculations. It is observed that the HOMO−LUMO energy difference for inhibitor 9 (3.77 eV) is higher than that of inhibitor 5 (3.40 eV). The HUMO energies for inhibitors 5 and 9 are nearly identical, but the LUMO energy for inhibitor 9 is higher than that for inhibitor 5. A higher energy LUMO suggests a more electron-deficient character of the heteroaryl C-ring leading to stabilization interaction with the serine (Ser936) residue of JAK2. In short, the electronegativity of F leads to the electrostatic pull of the hydrogen atom in the serine residue and is responsible for a higher residence time for inhibitor 9 than other inhibitors.

To gain additional insights into the dynamics of the receptor−inhibitor complex and to explain the discrepancy in residence times of inhibitor 5 and inhibitor 9 for the JAK2−inhibitor complex, PCA is implemented to the 3D positional coordinates obtained from the MD trajectories.[127−129] PCA explains the variance in the data set by transforming the MD trajectories into a set of orthogonal vectors or principal components representing characteristic molecular internal motions. The first PC shows the maximum variance in the data, followed by the second PC and so on. Although the first PC is extremely useful in gaining insights into the system dynamics, the actual motion of the system is the combination of all the PCs. Figure 9a and b shows the first PC obtained for the JAK2−inhibitor 5 and JAK2−inhibitor 9 complex, respectively. Figure 9a shows a greater domain movement around the binding region of the JAK2−inhibitor 5 complex. This motion may be attributed to a region of high instability around the binding site for inhibitor 5, leading to a lower residence time than inhibitor 9.

3.2.2. Selectivity of Inhibitors toward JAK2 over JAK3. The inhibitors at the binding site of the JAK2 protein display higher residence times than the same series of inhibitors for the JAK3 protein. To corroborate these experimental findings, minimum average distance analysis is performed to obtain a detailed description of the binding pocket of the JAK−inhibitor complex. The minimum distance between any two atoms of the amino acid and the inhibitor averaged over the course of the 2 μs trajectory for all the residues is calculated for the JAK−inhibitor complexes. Figure 10a represents the binding pocket of JAK2−inhibitor 9 complex, while Figure 10b represents the binding pocket of JAK3−inhibitor 9 complex. Interacting residues described in the figure are chosen with a cutoff distance of 4 Å. Table S4 shows the list of interacting residues for inhibitor 9 in complex with JAK2 and JAK3 proteins. It is evident from Figure 10a and b that inhibitor 9 interacts with more residues of JAK2 over JAK3. It is also observed that the binding site occupies a larger volume, and the inhibitor is placed deeper in the binding pocket of JAK2, explaining the selectivity of the same toward JAK2 over JAK3. Interestingly for JAK3, it has been observed that the substituted fluorine atom in the heteroaryl C-ring in inhibitor 9 does not interact with the hydrogen of the β-carbon or any other heavy atom of the serine residue (Ser907).

Root mean square fluctuations (RMSF) calculations are performed to identify important residues and domains associated with inhibitor binding and unbinding.[130] A root mean squared (RMS) fit to the average structure is performed to obtain the fluctuations without rotations and translations, and a mass-weighted averaging of atomic fluctuations for each residue is carried out for the entire simulation trajectory. As demonstrated in Figure 11a, the binding site flanking residues for JAK2, namely, Gly856, Lys857, Phe860, Gly861, Ser887,

https://doi.org/10.1021/acs.jcim.2c01589
J. Chem. Inf. Model. 2023, 63, 2469−2482

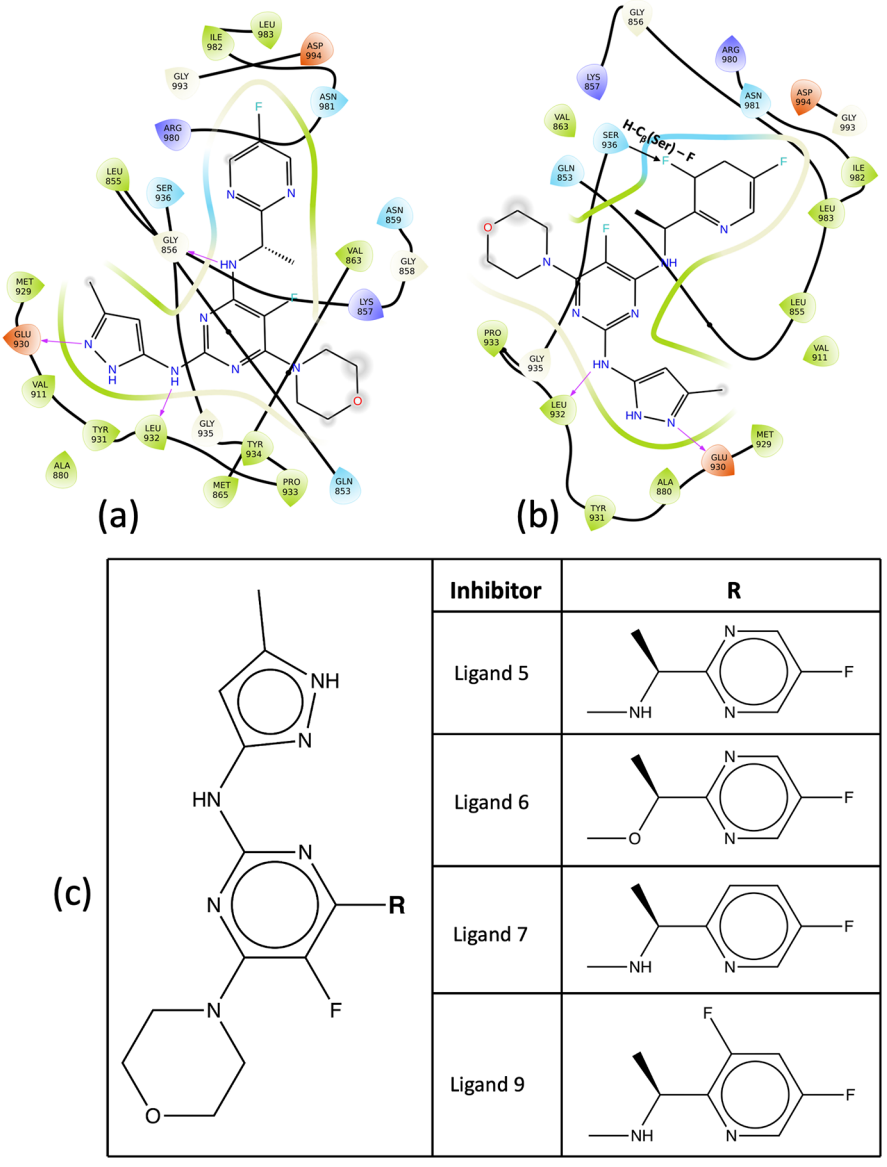

Figure 8. (a, b) Binding site of inhibitors for JAK2 complex showing important interactions with surrounding residues: (a) JAK2−inhibitor 5 complex and (b) JAK2−inhibitor 9 complex. (c) 2D formulas schemes for the JAK inhibitors indicating the location of modifications. In inhibitor 9, the substituted fluorine atom in the heteroaryl C-ring leads to the electrostatic pull of the hydrogen atom in the nearby serine residue, which contributes to the higher residence time in the kinase domain.

Glu889, Asp894, Arg897, Glu898, and Arg922, have lower RMSF values and stabilize upon inhibitor 9 binding as compared to inhibitor 5, suggesting their roles in stabilizing the receptor−inhibitor complex. Similarly, in JAK3 proteins, however, residue fluctuations are mostly similar, though only a few of the binding site flanking residues, such as Phe833, Gly834, Gln858, Gly861, Pro862, Asp863, Gln864, and Phe868, show a significant difference in fluctuations upon inhibitor 9 binding as compared to inhibitor 6 (Figure 11b). A higher number of residues in JAK2 contributing to the low fluctuations at the binding site may contribute to the selectivity of inhibitor 9 toward JAK2 over JAK3.

The binding pocket volumes of the JAKs are a direct consequence of residues interacting with the inhibitor at the ATP binding site. These pocket volumes are complementary to the shape of the inhibitors as well. To compare the binding pockets of different inhibitors in JAK2 and JAK3 proteins, POVME, a tool to analyze binding pocket volumes, was utilized.[131,132] POVME provides a grid-based pocket representation of the inhibitor binding site. The pocket volumes are calculated with a grid spacing of 0.1 Å and a distance cutoff of 1.09 Å. Deep pocket volumes are observed for the JAK2 inhibitors where these inhibitors are tightly bound to the interacting residues. Figure S1 shows a distinct difference in the binding pocket volumes for JAK2 vs JAK3 proteins, where the volumes associated with inhibitors in the binding domain of JAK2 are significantly higher than those of JAK3.

Inhibitor-binding site distance analysis is performed for each receptor−inhibitor complex averaged over three independent MD simulation trajectories of 2 μs each. From the starting structure of the zeroth milestone of each JAK−inhibitor complex, residues encompassing the inhibitor within a cutoff radius of 4 Å defined the binding site. The distance between the center of masses of the inhibitors and the α-C atoms of the binding site are used to calculate the inhibitor-binding site distance. It has been observed for all four inhibitors that the

https://doi.org/10.1021/acs.jcim.2c01589
J. Chem. Inf. Model. 2023, 63, 2469−2482

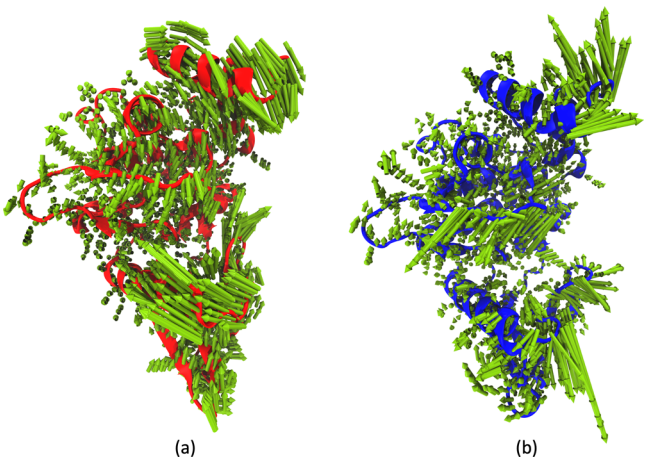

Figure 9. Principal component analysis for JAK2−inhibitor complexes from 2 μs of MD simulation trajectory: (a) First normal mode for JAK2−inhibitor 5 complex (47% of accounted variance). (b) First normal mode for JAK2−inhibitor 9 complex (46% of accounted variance).

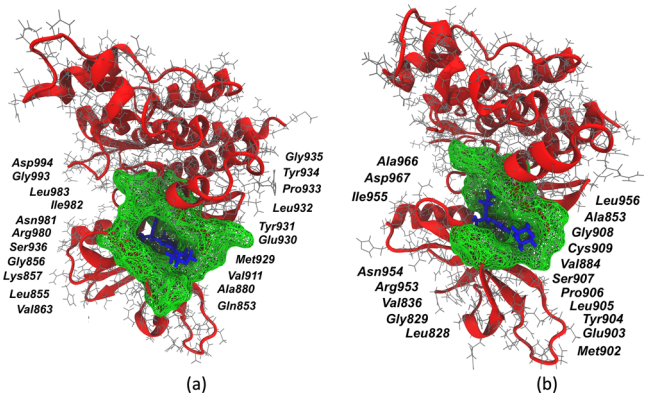

Figure 10. Binding site (green mesh) obtained from minimum average inhibitor−residue distances from three independent 2 μs of MD simulation trajectories: (a) JAK2−inhibitor 9 complex and (b) JAK3−inhibitor 9 complex.

inhibitor-binding site distance in the case of JAK2−inhibitor complexes is less than that of the JAK3−inhibitor complexes (Figure S2), suggesting strong binding of the inhibitors to the JAK2 protein.

JAK inhibitors target the JAK family of kinases and bind to the ATP-binding site of the kinase domain, thereby preventing the phosphorylation of downstream signaling proteins. In the case of JAK2 proteins, the backbone amide and carbonyl groups (Leu855, Met929, and Leu932) interact with the phosphate groups of the ATP, forming multiple hydrogen bonds.[133,134] These interactions at the hinge region are of particular interest as they are conserved in the case of JAK2−inhibitor interactions (Figure 1). The inhibitors contain a heterocyclic core that mimics the adenine ring of the ATP to retain such interactions. Additionally, other interactions of these inhibitors with the kinase domain lead to the selectivity of these inhibitors over other kinases (Figure 8a and b).

4. CONCLUSION

The SEEKR2 milestoning method proved efficient in estimating the experimental residence times for different JAK−inhibitor complexes. The trend in residence times for the set of inhibitors for the JAK2 and JAK3 proteins is also conserved. It becomes evident from the SEEKR2 milestoning approach and the experiments that the series of inhibitors display an extended residence time and bind stronger to JAK2 than to JAK3. Among the inhibitors, inhibitor 9 displayed the highest residence time in the JAK2 protein. The results are further supported by MD simulations where important binding residues have lower distances from the inhibitor and less fluctuation in the JAK2−inhibitor 9 complex. In addition, the QM calculations show a higher electron density on the fluorine groups in the heteroaryl C-ring of inhibitor 9, strengthening the binding with JAK2 and JAK3 proteins resulting in the highest residence time among all the inhibitors. SEEKR2 thereby proves to be a valuable tool to predict the kinetics and thermodynamics of receptor−ligand binding and unbinding as it is user friendly, requires minimum structural information on the system, is embarrassingly parallel, and requires a comparatively short simulation time to reach converged kinetic rates.

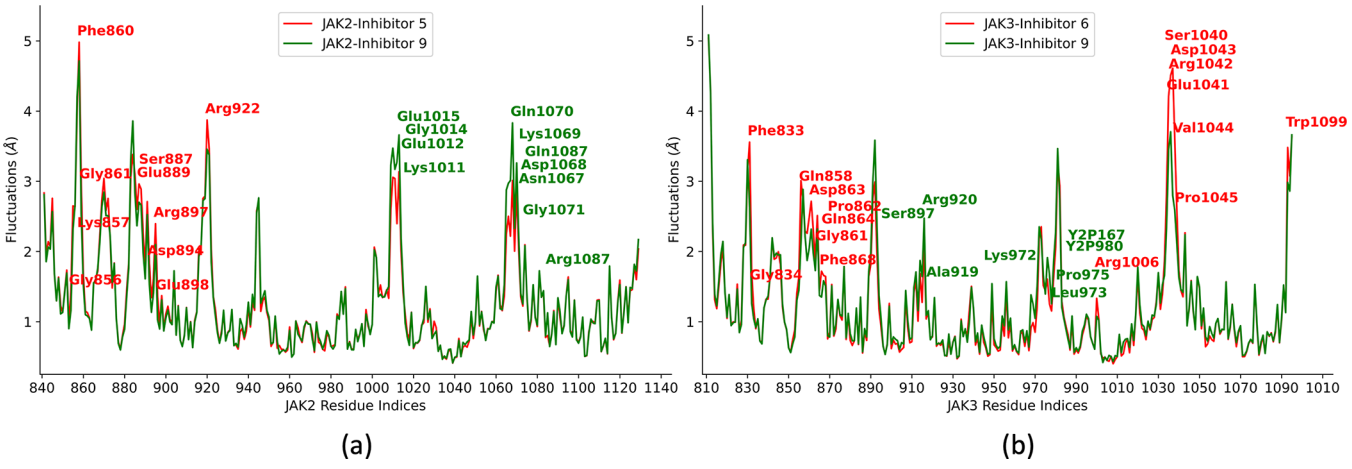

Figure 11. Residue fluctuation analysis for JAK2 and JAK3−inhibitor complexes obtained from three independent 2 μs of MD simulation trajectories: (a) JAK2−inhibitor 5 vs JAK2−inhibitor 9 complex and (b) JAK3−inhibitor 6 vs JAK3−inhibitor 9 complex

https://doi.org/10.1021/acs.jcim.2c01589
J. Chem. Inf. Model. 2023, 63, 2469−2482

■ ASSOCIATED CONTENT

Data Availability Statement

The SEEKR2 project is available at https://github.com/seekrcentral/seekr2. The structures of JAK2 and JAK3 proteins complexed with the inhibitors, analysis scripts, and scripts for system preparations for SEEKR2 simulations are available at https://github.com/anandojha/kinase_SEEKR. The data for this study can be found at https://doi.org/10.6075/J01Z44MN.

Supporting Information

The Supporting Information is available free of charge at https://pubs.acs.org/doi/10.1021/acs.jcim.2c01589.

List of interacting residues of JAKs with inhibitors, pocket volume analysis, and inhibitor-binding site analysis for different JAK−inhibitor complexes (PDF)

■ AUTHOR INFORMATION

Corresponding Author

Rommie E. Amaro − *Department of Chemistry and Biochemistry, University of California San Diego, La Jolla, California 92093, United States;* orcid.org/0000-0002-9275-9553; Email: ramaro@ucsd.edu

Authors

Anupam Anand Ojha − *Department of Chemistry and Biochemistry, University of California San Diego, La Jolla, California 92093, United States;* orcid.org/0000-0001-6588-3092

Ambuj Srivastava − *Department of Chemistry and Biochemistry, University of California San Diego, La Jolla, California 92093, United States*

Lane William Votapka − *Department of Chemistry and Biochemistry, University of California San Diego, La Jolla, California 92093, United States;* orcid.org/0000-0002-0865-5867

Complete contact information is available at: https://pubs.acs.org/10.1021/acs.jcim.2c01589

Notes

The authors declare no competing financial interest.

■ ACKNOWLEDGMENTS

The authors acknowledge Benjamin Jagger and Shiksha Dutta for insightful and helpful discussions. A.A.O. acknowledges the support of the Molecular Sciences Software Institute (MolSSI) fellowship under NSF Grant OAC-1547580. R.E.A. acknowledges support from NSF Extreme Science and Engineering Discovery Environment (XSEDE) CHE060063 and NIH GM132826. All simulations were performed using the Triton Shared Computing Cluster (TSCC) and Popeye computing cluster at the San Diego Supercomputing Center (SDSC).

■ REFERENCES

(1) Hunter, T.; Cooper, J. A. Protein-tyrosine kinases. *Annual review of biochemistry* **1985**, *54*, 897−930.

(2) Schlessinger, J. Cell signaling by receptor tyrosine kinases. *Cell* **2000**, *103*, 211−225.

(3) Pawson, T. Regulation and targets of receptor tyrosine kinases. *European journal of cancer* **2002**, *38*, S3−S10.

(4) Lemmon, M. A.; Schlessinger, J. Cell signaling by receptor tyrosine kinases. *Cell* **2010**, *141*, 1117−1134.

(5) Taniguchi, T. Cytokine signaling through nonreceptor protein tyrosine kinases. *Science* **1995**, *268*, 251−255.

(6) Ghoreschi, K.; Laurence, A.; O'Shea, J. J. Janus kinases in immune cell signaling. *Immunological Reviews* **2009**, *228*, 273−287.

(7) Yamaoka, K.; Saharinen, P.; Pesu, M.; Holt, V. E.; Silvennoinen, O.; O'Shea, J. J. The janus kinases (jaks). *Genome Biology* **2004**, *5*, 1−6.

(8) Hochhaus, A. Protein Tyrosine Kinases. From Inhibitors to Useful Drugs. *Leukemia* **2006**, *20*, 1465.

(9) Imada, K.; Leonard, W. J. The jak-STAT pathway. *Molecular immunology* **2000**, *37*, 1−11.

(10) Gao, B. Cytokines, STATs and liver disease. *Cell Mol. Immunol* **2005**, *2*, 92−100.

(11) Xin, P.; Xu, X.; Deng, C.; Liu, S.; Wang, Y.; Zhou, X.; Ma, H.; Wei, D.; Sun, S. The role of JAK/STAT signaling pathway and its inhibitors in diseases. *International immunopharmacology* **2020**, *80*, 106210.

(12) O'Shea, J. J.; Schwartz, D. M.; Villarino, A. V.; Gadina, M.; McInnes, I. B.; Laurence, A. The JAK-STAT pathway: impact on human disease and therapeutic intervention. *Annual review of medicine* **2015**, *66*, 311−328.

(13) Morris, R.; Kershaw, N. J.; Babon, J. J. The molecular details of cytokine signaling via the JAK/STAT pathway. *Protein Sci.* **2018**, *27*, 1984−2009.

(14) Rawlings, J. S.; Rosler, K. M.; Harrison, D. A. The JAK/STAT signaling pathway. *Journal of cell science* **2004**, *117*, 1281−1283.

(15) Giordanetto, F.; Kroemer, R. T. Prediction of the structure of human Janus kinase 2 (JAK2) comprising JAK homology domains 1 through 7. *Protein engineering* **2002**, *15*, 727−737.

(16) Lo, Y.-C.; Liu, T.; Morrissey, K. M.; Kakiuchi-Kiyota, S.; Johnson, A. R.; Broccatelli, F.; Zhong, Y.; Joshi, A.; Altman, R. B. Computational analysis of kinase inhibitor selectivity using structural knowledge. *Bioinformatics* **2019**, *35*, 235−242.

(17) Haan, C.; Kreis, S.; Margue, C.; Behrmann, I. Jaks and cytokine receptors—an intimate relationship. *Biochemical pharmacology* **2006**, *72*, 1538−1546.

(18) Sriram, K.; Benkovic, S. A.; Hebert, M. A.; Miller, D. B.; O'Callaghan, J. P. Induction of gp130-related cytokines and activation of JAK2/STAT3 pathway in astrocytes precedes up-regulation of glial fibrillary acidic protein in the 1-methyl-4-phenyl-1, 2, 3, 6-tetrahydropyridine model of neurodegeneration: key signaling pathway for astrogliosis in vivo? *J. Biol. Chem.* **2004**, *279*, 19936−19947.

(19) Watanabe, S.; Itoh, T.; Arai, K.-i. Roles of JAK kinases in human GM-CSF receptor signal transduction. *Journal of allergy and clinical immunology* **1996**, *98*, S183−S191.

(20) Hubbard, S. R. Mechanistic insights into regulation of JAK2 tyrosine kinase. *Frontiers in endocrinology* **2018**, *8*, 361.

(21) Suzuki, K.; Nakajima, H.; Saito, Y.; Saito, T.; Leonard, W. J.; Iwamoto, I. Janus kinase 3 (Jak3) is essential for common cytokine receptor γ chain (γc)-dependent signaling: comparative analysis of γc, Jak3, and γc and Jak3 double-deficient mice. *International immunology* **2000**, *12*, 123−132.

(22) Koppikar, P.; Bhagwat, N.; Kilpivaara, O.; Manshouri, T.; Adli, M.; Hricik, T.; Liu, F.; Saunders, L. M.; Mullally, A.; Abdel-Wahab, O.; et al. Heterodimeric JAK−STAT activation as a mechanism of persistence to JAK2 inhibitor therapy. *Nature* **2012**, *489*, 155−159.

(23) Verstovsek, S.; Mesa, R. A.; Gotlib, J.; Levy, R. S.; Gupta, V.; DiPersio, J. F.; Catalano, J. V.; Deininger, M.; Miller, C.; Silver, R. T.; et al. A double-blind, placebo-controlled trial of ruxolitinib for myelofibrosis. *New England Journal of Medicine* **2012**, *366*, 799−807.

(24) Schwartz, D. M.; Kanno, Y.; Villarino, A.; Ward, M.; Gadina, M.; O'Shea, J. J. JAK inhibition as a therapeutic strategy for immune and inflammatory diseases. *Nat. Rev. Drug Discovery* **2017**, *16*, 843−862.

(25) Fleischmann, R.; Cutolo, M.; Genovese, M. C.; Lee, E. B.; Kanik, K. S.; Sadis, S.; Connell, C. A.; Gruben, D.; Krishnaswami, S.; Wallenstein, G.; et al. Phase IIb dose-ranging study of the oral JAK inhibitor tofacitinib (CP-690,550) or adalimumab monotherapy

versus placebo in patients with active rheumatoid arthritis with an inadequate response to disease-modifying antirheumatic drugs. *Arthritis & Rheumatism* **2012**, *64*, 617−629.
(26) Ghoreschi, K.; Jesson, M. I.; Li, X.; Lee, J. L.; Ghosh, S.; Alsup, J. W.; Warner, J. D.; Tanaka, M.; Steward-Tharp, S. M.; Gadina, M.; et al. Modulation of innate and adaptive immune responses by tofacitinib (CP-690,550). *J. Immunol.* **2011**, *186*, 4234−4243.
(27) Sandborn, W. J.; Ghosh, S.; Panes, J.; Vranic, I.; Su, C.; Rousell, S.; Niezychowski, W. Tofacitinib, an oral Janus kinase inhibitor, in active ulcerative colitis. *New England Journal of Medicine* **2012**, *367*, 616−624.
(28) Danese, S.; Grisham, M.; Hodge, J.; Telliez, J.-B. JAK inhibition using tofacitinib for inflammatory bowel disease treatment: a hub for multiple inflammatory cytokines. *American Journal of Physiology-Gastrointestinal and Liver Physiology* **2016**, *310*, G155−G162.
(29) Vyas, D.; O'Dell, K. M.; Bandy, J. L.; Boyce, E. G. Tofacitinib: The First Janus Kinase (JAK) inhibitor for the treatment of rheumatoid arthritis. *Annals of Pharmacotherapy* **2013**, *47*, 1524−1531.
(30) Mogul, A.; Corsi, K.; McAuliffe, L. Baricitinib: the second FDA-approved JAK inhibitor for the treatment of rheumatoid arthritis. *Annals of Pharmacotherapy* **2019**, *53*, 947−953.
(31) Menet, C. J.; Van Rompaey, L.; Geney, R. Advances in the discovery of selective JAK inhibitors. *Progress in Medicinal Chemistry* **2013**, *52*, 153−223.
(32) Adcock, S. A.; McCammon, J. A. Molecular dynamics: survey of methods for simulating the activity of proteins. *Chem. Rev.* **2006**, *106*, 1589−1615.
(33) Lindahl, E.; Sansom, M. S. Membrane proteins: molecular dynamics simulations. *Curr. Opin. Struct. Biol.* **2008**, *18*, 425−431.
(34) Karplus, M.; McCammon, J. A. Molecular dynamics simulations of biomolecules. *Nature structural biology* **2002**, *9*, 646−652.
(35) Swope, W. C.; Pitera, J. W.; Suits, F. Describing protein folding kinetics by molecular dynamics simulations. 1. Theory. *J. Phys. Chem. B* **2004**, *108*, 6571−6581.
(36) Mollica, L.; Decherchi, S.; Zia, S. R.; Gaspari, R.; Cavalli, A.; Rocchia, W. Kinetics of protein-ligand unbinding via smoothed potential molecular dynamics simulations. *Sci. Rep.* **2015**, *5*, 11539.
(37) Wolf, S.; Amaral, M.; Lowinski, M.; Vallée, F.; Musil, D.; Guldenhaupt, J.; Dreyer, M. K.; Bomke, J.; Frech, M.; Schlitter, J.; et al. Estimation of protein−ligand unbinding kinetics using non-equilibrium targeted molecular dynamics simulations. *J. Chem. Inf. Model.* **2019**, *59*, 5135−5147.
(38) Spiriti, J.; Noé, F.; Wong, C. F. Simulation of ligand dissociation kinetics from the protein kinase PYK2. *Journal of computational chemistry* **2022**, *43*, 1911−1922.
(39) Plattner, N.; Noé, F. Protein conformational plasticity and complex ligand-binding kinetics explored by atomistic simulations and Markov models. *Nat. Commun.* **2015**, *6*, 1−10.
(40) Kokh, D. B.; Amaral, M.; Bomke, J.; Gradler, U.; Musil, D.; Buchstaller, H.-P.; Dreyer, M. K.; Frech, M.; Lowinski, M.; Vallee, F.; et al. Estimation of drug-target residence times by τ-random acceleration molecular dynamics simulations. *J. Chem. Theory Comput.* **2018**, *14*, 3859−3869.
(41) Bernetti, M.; Masetti, M.; Rocchia, W.; Cavalli, A. Kinetics of drug binding and residence time. *Annu. Rev. Phys. Chem.* **2019**, *70*, 143−171.
(42) Tiwary, P.; Mondal, J.; Berne, B. J. How and when does an anticancer drug leave its binding site? *Science Advances* **2017**, *3*, No. e1700014.
(43) Tiwary, P.; Limongelli, V.; Salvalaglio, M.; Parrinello, M. Kinetics of protein−ligand unbinding: Predicting pathways, rates, and rate-limiting steps. *Proc. Natl. Acad. Sci. U. S. A.* **2015**, *112*, E386−E391.
(44) Bernetti, M.; Cavalli, A.; Mollica, L. Protein−ligand (un) binding kinetics as a new paradigm for drug discovery at the crossroad between experiments and modelling. *MedChemComm* **2017**, *8*, 534−550.
(45) Fang, Y. Ligand−receptor interaction platforms and their applications for drug discovery. *Expert opinion on drug discovery* **2012**, *7*, 969−988.
(46) Renaud, J.-P.; Chung, C.-w.; Danielson, U. H.; Egner, U.; Hennig, M.; Hubbard, R. E.; Nar, H. Biophysics in drug discovery: impact, challenges and opportunities. *Nat. Rev. Drug Discovery* **2016**, *15*, 679−698.
(47) Copeland, R. A.; Pompliano, D. L.; Meek, T. D. Drug−target residence time and its implications for lead optimization. *Nat. Rev. Drug Discovery* **2006**, *5*, 730−739.
(48) Copeland, R. A. The drug−target residence time model: a 10-year retrospective. *Nat. Rev. Drug Discovery* **2016**, *15*, 87−95.
(49) Lu, H.; Tonge, P. J. Drug−target residence time: critical information for lead optimization. *Curr. Opin. Chem. Biol.* **2010**, *14*, 467−474.
(50) Zhang, R.; Monsma, F. The importance of drug-target residence time. *Curr. Opin. Drug Discov. Devel.* **2009**, *12*, 488−496.
(51) Sousa, S. F.; Fernandes, P. A.; Ramos, M. J. Protein−ligand docking: current status and future challenges. *Proteins: Struct., Funct., Bioinf.* **2006**, *65*, 15−26.
(52) Erickson, J. A.; Jalaie, M.; Robertson, D. H.; Lewis, R. A.; Vieth, M. Lessons in molecular recognition: the effects of ligand and protein flexibility on molecular docking accuracy. *Journal of medicinal chemistry* **2004**, *47*, 45−55.
(53) Nayeem, A.; Krystek, S., Jr.; Stouch, T. An assessment of protein−ligand binding site polarizability. *Biopolymers: Original Research on Biomolecules* **2003**, *70*, 201−211.
(54) Goel, H.; Yu, W.; Ustach, V. D.; Aytenfisu, A. H.; Sun, D.; MacKerell, A. D. Impact of electronic polarizability on protein-functional group interactions. *Phys. Chem. Chem. Phys.* **2020**, *22*, 6848−6860.
(55) Andersen, B. F.; Baker, H. M.; Morris, G. E.; Rumball, S. V.; Baker, E. N. Apolactoferrin structure demonstrates ligand-induced conformational change in transferrins. *Nature* **1990**, *344*, 784−787.
(56) Ha, T.; Zhuang, X.; Kim, H. D.; Orr, J. W.; Williamson, J. R.; Chu, S. Ligand-induced conformational changes observed in single RNA molecules. *Proc. Natl. Acad. Sci. U. S. A.* **1999**, *96*, 9077−9082.
(57) Ahmad, E.; Rabbani, G.; Zaidi, N.; Khan, M. A.; Qadeer, A.; Ishtikhar, M.; Singh, S.; Khan, R. H. Revisiting ligand-induced conformational changes in proteins: essence, advancements, implications and future challenges. *J. Biomol. Struct. Dyn.* **2013**, *31*, 630−648.
(58) Tiwary, P.; Parrinello, M. From metadynamics to dynamics. *Physical review letters* **2013**, *111*, 230602.
(59) Clark, A. J.; Tiwary, P.; Borrelli, K.; Feng, S.; Miller, E. B.; Abel, R.; Friesner, R. A.; Berne, B. J. Prediction of protein−ligand binding poses via a combination of induced fit docking and metadynamics simulations. *J. Chem. Theory Comput.* **2016**, *12*, 2990−2998.
(60) Casasnovas, R.; Limongelli, V.; Tiwary, P.; Carloni, P.; Parrinello, M. Unbinding kinetics of a p38 MAP kinase type II inhibitor from metadynamics simulations. *J. Am. Chem. Soc.* **2017**, *139*, 4780−4788.
(61) Shekhar, M.; Smith, Z.; Seeliger, M. A.; Tiwary, P. Protein flexibility and dissociation pathway differentiation can explain onset of resistance mutations in kinases. *Angew. Chem., Int. Ed.* **2022**, *61*, No. e202200983.
(62) Sutto, L.; Marsili, S.; Gervasio, F. L. New advances in metadynamics. *Wiley Interdisciplinary Reviews: Computational Molecular Science* **2012**, *2*, 771−779.
(63) Comer, J.; Gumbart, J. C.; Hénin, J.; Lelièvre, T.; Pohorille, A.; Chipot, C. The adaptive biasing force method: Everything you always wanted to know but were afraid to ask. *J. Phys. Chem. B* **2015**, *119*, 1129−1151.
(64) Martin, H. S.; Jha, S.; Coveney, P. V. Comparative analysis of nucleotide translocation through protein nanopores using steered molecular dynamics and an adaptive biasing force. *Journal of computational chemistry* **2014**, *35*, 692−702.
(65) Lelièvre, T.; Rousset, M.; Stoltz, G. Long-time convergence of an adaptive biasing force method. *Nonlinearity* **2008**, *21*, 1155.

https://doi.org/10.1021/acs.jcim.2c01589
J. Chem. Inf. Model. 2023, 63, 2469−2482

(66) Kästner, J. Umbrella sampling. *Wiley Interdisciplinary Reviews: Computational Molecular Science* **2011**, *1*, 932−942.
(67) Virnau, P.; Müller, M. Calculation of free energy through successive umbrella sampling. *J. Chem. Phys.* **2004**, *120*, 10925−10930.
(68) Wang, J.; Arantes, P. R.; Bhattarai, A.; Hsu, R. V.; Pawnikar, S.; Huang, Y.-m. M.; Palermo, G.; Miao, Y. Gaussian accelerated molecular dynamics: Principles and applications. *Wiley Interdisciplinary Reviews: Computational Molecular Science* **2021**, *11*, No. e1521.
(69) Miao, Y.; McCammon, J. A. *Annual Reports in Computational Chemistry*; Elsevier, 2017; Vol. *13*; pp 231−278.
(70) Miao, Y.; Bhattarai, A.; Wang, J. Ligand Gaussian accelerated molecular dynamics (LiGaMD): Characterization of ligand binding thermodynamics and kinetics. *J. Chem. Theory Comput.* **2020**, *16*, 5526−5547.
(71) Wang, J.; Miao, Y. Ligand Gaussian Accelerated Molecular Dynamics 2 (LiGaMD2): Improved Calculations of Ligand Binding Thermodynamics and Kinetics with Closed Protein Pocket. *J. Chem. Theory Comput.* **2023**, *19*, 733−745.
(72) Kokh, D. B.; Kaufmann, T.; Kister, B.; Wade, R. C. Machine learning analysis of τRAMD trajectories to decipher molecular determinants of drug-target residence times. *Frontiers in Molecular Biosciences* **2019**, *6*, 36.
(73) Ahinko, M.; Niinivehmas, S.; Jokinen, E.; Pentikäinen, O. T. Suitability of MMGBSA for the selection of correct ligand binding modes from docking results. *Chemical Biology & Drug Design* **2019**, *93*, 522−538.
(74) Woo, H.-J.; Roux, B. Calculation of absolute protein−ligand binding free energy from computer simulations. *Proc. Natl. Acad. Sci. U. S. A.* **2005**, *102*, 6825−6830.
(75) Doudou, S.; Burton, N. A.; Henchman, R. H. Standard free energy of binding from a one-dimensional potential of mean force. *J. Chem. Theory Comput.* **2009**, *5*, 909−918.
(76) Gumbart, J. C.; Roux, B.; Chipot, C. Standard binding free energies from computer simulations: What is the best strategy? *J. Chem. Theory Comput.* **2013**, *9*, 794−802.
(77) Elber, R. A new paradigm for atomically detailed simulations of kinetics in biophysical systems. *Q. Rev. Biophys.* **2017**, *50*, No. e8.
(78) Doerr, S.; De Fabritiis, G. On-the-fly learning and sampling of ligand binding by high-throughput molecular simulations. *J. Chem. Theory Comput.* **2014**, *10*, 2064−2069.
(79) Prinz, J.-H.; Wu, H.; Sarich, M.; Keller, B.; Senne, M.; Held, M.; Chodera, J. D.; Schütte, C.; Noé, F. Markov models of molecular kinetics: Generation and validation. *J. Chem. Phys.* **2011**, *134*, 174105.
(80) Bernetti, M.; Masetti, M.; Recanatini, M.; Amaro, R. E.; Cavalli, A. An integrated Markov state model and path metadynamics approach to characterize drug binding processes. *J. Chem. Theory Comput.* **2019**, *15*, 5689−5702.
(81) Amaro, R. E.; Mulholland, A. J. Multiscale methods in drug design bridge chemical and biological complexity in the search for cures. *Nature Reviews Chemistry* **2018**, *2*, 0148.
(82) Gobbo, D.; Piretti, V.; Di Martino, R. M. C.; Tripathi, S. K.; Giabbai, B.; Storici, P.; Demitri, N.; Girotto, S.; Decherchi, S.; Cavalli, A. Investigating drug−target residence time in kinases through enhanced sampling simulations. *J. Chem. Theory Comput.* **2019**, *15*, 4646−4659.
(83) Sun, H.; Tian, S.; Zhou, S.; Li, Y.; Li, D.; Xu, L.; Shen, M.; Pan, P.; Hou, T. Revealing the favorable dissociation pathway of type II kinase inhibitors via enhanced sampling simulations and two-end-state calculations. *Sci. Rep.* **2015**, *5*, 8457.
(84) Guan, H.; Lamb, M. L.; Peng, B.; Huang, S.; DeGrace, N.; Read, J.; Hussain, S.; Wu, J.; Rivard, C.; Alimzhanov, M.; et al. Discovery of novel Jak2−Stat pathway inhibitors with extended residence time on target. *Bioorganic & medicinal chemistry letters* **2013**, *23*, 3105−3110.
(85) Barducci, A.; Bonomi, M.; Parrinello, M. Metadynamics. *Wiley Interdisciplinary Reviews: Computational Molecular Science* **2011**, *1*, 826−843.
(86) Ahn, S.-H.; Ojha, A. A.; Amaro, R. E.; McCammon, J. A. Gaussian-Accelerated Molecular Dynamics with the Weighted Ensemble Method: A Hybrid Method Improves Thermodynamic and Kinetic Sampling. *J. Chem. Theory Comput.* **2021**, *17*, 7938−7951.
(87) Bernardi, R. C.; Melo, M. C.; Schulten, K. Enhanced sampling techniques in molecular dynamics simulations of biological systems. *Biochimica et Biophysica Acta (BBA)-General Subjects* **2015**, *1850*, 872−877.
(88) Zwier, M. C.; Adelman, J. L.; Kaus, J. W.; Pratt, A. J.; Wong, K. F.; Rego, N. B.; Suárez, E.; Lettieri, S.; Wang, D. W.; Grabe, M.; et al. WESTPA: An interoperable, highly scalable software package for weighted ensemble simulation and analysis. *J. Chem. Theory Comput.* **2015**, *11*, 800−809.
(89) Mardt, A.; Pasquali, L.; Wu, H.; Noé, F. VAMPnets for deep learning of molecular kinetics. *Nat. Commun.* **2018**, *9*, 1−11.
(90) Ojha, A. A.; Thakur, S.; Ahn, S.-H.; Amaro, R. E. DeepWEST: Deep learning of kinetic models with the Weighted Ensemble Simulation Toolkit for enhanced sampling. *J. Chem. Theory Comput.* **2023**, *19*, 1342−1359.
(91) Du, Q.; Faber, V.; Gunzburger, M. Centroidal Voronoi tessellations: Applications and algorithms. *SIAM review* **1999**, *41*, 637−676.
(92) Møller, J. *Lectures on Random Voronoi Tessellations*; Springer Science & Business Media, 2012; Vol. *87*.
(93) Votapka, L. W.; Jagger, B. R.; Heyneman, A. L.; Amaro, R. E. SEEKR: simulation enabled estimation of kinetic rates, a computational tool to estimate molecular kinetics and its application to trypsin−benzamidine binding. *J. Phys. Chem. B* **2017**, *121*, 3597−3606.
(94) Votapka, L. W.; Stokely, A. M.; Ojha, A. A.; Amaro, R. E. SEEKR2: Versatile multiscale milestoning utilizing the OpenMM molecular dynamics engine. *J. Chem. Inf. Model.* **2022**, *62*, 3253−3262.
(95) Jagger, B. R.; Ojha, A. A.; Amaro, R. E. Predicting ligand binding kinetics using a Markovian milestoning with voronoi tessellations multiscale approach. *J. Chem. Theory Comput.* **2020**, *16*, 5348−5357.
(96) Huber, G. A.; McCammon, J. A. Browndye: a software package for Brownian dynamics. *Comput. Phys. Commun.* **2010**, *181*, 1896−1905.
(97) Izrailev, S.; Stepaniants, S.; Isralewitz, B.; Kosztin, D.; Lu, H.; Molnar, F.; Wriggers, W.; Schulten, K. *Computational Molecular Dynamics: Challenges, Methods, Ideas*; Springer, 1999; pp 39−65.
(98) Vanden-Eijnden, E.; Venturoli, M. Markovian milestoning with Voronoi tessellations. *J. Chem. Phys.* **2009**, *130*, 194101.
(99) West, A. M.; Elber, R.; Shalloway, D. Extending molecular dynamics time scales with milestoning: Example of complex kinetics in a solvated peptide. *J. Chem. Phys.* **2007**, *126*, 145104.
(100) Bian, M.; Ma, Q.-q.; Wu, Y.; Du, H.-h.; Guo-Hua, G. Small molecule compounds with good anti-inflammatory activity reported in the literature from 01/2009 to 05/2021: a review. *Journal of Enzyme Inhibition and Medicinal Chemistry* **2021**, *36*, 2139−2159.
(101) Copeland, R. A. *Evaluation of Enzyme Inhibitors in Drug Discovery: A Guide for Medicinal Chemists and Pharmacologists*; John Wiley & Sons, 2013.
(102) Madhavi Sastry, G.; Adzhigirey, M.; Day, T.; Annabhimoju, R.; Sherman, W. Protein and ligand preparation: parameters, protocols, and influence on virtual screening enrichments. *Journal of computer-aided molecular design* **2013**, *27*, 221−234.
(103) Wang, J.; Wolf, R. M.; Caldwell, J. W.; Kollman, P. A.; Case, D. A. Development and testing of a general amber force field. *Journal of computational chemistry* **2004**, *25*, 1157−1174.
(104) Maier, J. A.; Martinez, C.; Kasavajhala, K.; Wickstrom, L.; Hauser, K. E.; Simmerling, C. ff14SB: improving the accuracy of protein side chain and backbone parameters from ff99SB. *J. Chem. Theory Comput.* **2015**, *11*, 3696−3713.
(105) Jakalian, A.; Bush, B. L.; Jack, D. B.; Bayly, C. I. Fast, efficient generation of high-quality atomic charges. AM1-BCC model: I. Method. *Journal of computational chemistry* **2000**, *21*, 132−146.

https://doi.org/10.1021/acs.jcim.2c01589
J. Chem. Inf. Model. 2023, 63, 2469−2482

(106) Jakalian, A.; Jack, D. B.; Bayly, C. I. Fast, efficient generation of high-quality atomic charges. AM1-BCC model: II. Parameterization and validation. *Journal of computational chemistry* **2002**, *23*, 1623−1641.
(107) Horn, H. W.; Swope, W. C.; Pitera, J. W.; Madura, J. D.; Dick, T. J.; Hura, G. L.; Head-Gordon, T. Development of an improved four-site water model for biomolecular simulations: TIP4P-Ew. *J. Chem. Phys.* **2004**, *120*, 9665−9678.
(108) Eastman, P.; Swails, J.; Chodera, J. D.; McGibbon, R. T.; Zhao, Y.; Beauchamp, K. A.; Wang, L.-P.; Simmonett, A. C.; Harrigan, M. P.; Stern, C. D.; et al. OpenMM 7: Rapid development of high performance algorithms for molecular dynamics. *PLoS computational biology* **2017**, *13*, No. e1005659.
(109) Eastman, P.; Pande, V. OpenMM: A hardware-independent framework for molecular simulations. *Computing in science & engineering* **2010**, *12*, 34−39.
(110) Lynch, S. M.; DeVicente, J.; Hermann, J. C.; Jaime-Figueroa, S.; Jin, S.; Kuglstatter, A.; Li, H.; Lovey, A.; Menke, J.; Niu, L.; et al. Strategic use of conformational bias and structure based design to identify potent JAK3 inhibitors with improved selectivity against the JAK family and the kinome. *Bioorganic & medicinal chemistry letters* **2013**, *23*, 2793−2800.
(111) Dodda, L. S.; Tirado-Rives, J.; Jorgensen, W. L. Unbinding dynamics of non-nucleoside inhibitors from HIV-1 reverse transcriptase. *J. Phys. Chem. B* **2019**, *123*, 1741−1748.
(112) Ahmad, K.; Rizzi, A.; Capelli, R.; Mandelli, D.; Lyu, W.; Carloni, P. Enhanced-Sampling Simulations for the Estimation of Ligand Binding Kinetics: Current Status and Perspective. *Frontiers in molecular biosciences* **2022**, *9*, na DOI: 10.3389/fmolb.2022.899805.
(113) Dickson, A.; Tiwary, P.; Vashisth, H. Kinetics of ligand binding through advanced computational approaches: a review. *Current topics in medicinal chemistry* **2017**, *17*, 2626−2641.
(114) Case, D. A.; Cheatham, T. E., III; Darden, T.; Gohlke, H.; Luo, R.; Merz, K. M., Jr; Onufriev, A.; Simmerling, C.; Wang, B.; Woods, R. J. The Amber biomolecular simulation programs. *Journal of computational chemistry* **2005**, *26*, 1668−1688.
(115) Salomon-Ferrer, R.; Case, D. A.; Walker, R. C. An overview of the Amber biomolecular simulation package. *Wiley Interdisciplinary Reviews: Computational Molecular Science* **2013**, *3*, 198−210.
(116) Roe, D. R.; Cheatham, T. E., III PTRAJ and CPPTRAJ: software for processing and analysis of molecular dynamics trajectory data. *J. Chem. Theory Comput.* **2013**, *9*, 3084−3095.
(117) Chrencik, J. E.; Patny, A.; Leung, I. K.; Korniski, B.; Emmons, T. L.; Hall, T.; Weinberg, R. A.; Gormley, J. A.; Williams, J. M.; Day, J. E.; et al. Structural and thermodynamic characterization of the TYK2 and JAK3 kinase domains in complex with CP-690550 and CMP-6. *Journal of molecular biology* **2010**, *400*, 413−433.
(118) O'Shea, J. J.; Kontzias, A.; Yamaoka, K.; Tanaka, Y.; Laurence, A. Janus kinase inhibitors in autoimmune diseases. *Annals of the rheumatic diseases* **2013**, *72*, ii111−ii115.
(119) Vainchenker, W.; Kralovics, R. Genetic basis and molecular pathophysiology of classical myeloproliferative neoplasms. *Blood, The Journal of the American Society of Hematology* **2017**, *129*, 667−679.
(120) Tonge, P. J. Drug−target kinetics in drug discovery. *ACS chemical neuroscience* **2018**, *9*, 29−39.
(121) Daryaee, F.; Tonge, P. J. Pharmacokinetic−pharmacodynamic models that incorporate drug−target binding kinetics. *Curr. Opin. Chem. Biol.* **2019**, *50*, 120−127.
(122) Davoodi, S.; Daryaee, F.; Chang, A.; Walker, S. G.; Tonge, P. J. Correlating Drug−Target Residence Time and Post-antibiotic Effect: Insight into Target Vulnerability. *ACS infectious diseases* **2020**, *6*, 629−636.
(123) Frisch, M. J.; Trucks, G. W.; Schlegel, H. B.; Scuseria, G. E.; Robb, M. A.; Cheeseman, J. R.; Scalmani, G.; Barone, V.; Petersson, G. A.; Nakatsuji, H.; Li, X.; Caricato, M.; Marenich, A. V.; Bloino, J.; Janesko, B. G.; Gomperts, R.; Mennucci, B.; Hratchian, H. P.; Ortiz, J. V.; Izmaylov, A. F.; Sonnenber, J. L.; Williams-Young, D.; Ding, F.; Lipparini, F.; Egidi, F.; Goings, J.; Peng, B.; Petrone, A.; Henderson, T.; Ranasinghe, D.; Zakrzewsk, V. G.; Gao, J.; Rega, N.; Zheng, G.; Liang, W.; Hada, M.; Ehara, M.; Toyota, K.; Fukuda, R.; Hasegawa, J.; Ishida, M.; Nakajima, T.; Honda, Y.; Kitao, O.; Nakai, H; Vreven, T.; Throssell, K.; Montgomery, J. A., Jr.; Peralta, J. E.; Ogliaro, F.; Bearpark, M. J.; Heyd, J. J.; Brothers, E. N..; Kudin, K. N.; Staroverov, V. N.; Keith, T. A.; Kobayashi, R.; Normand, J.; Raghavachari, K.; Rendell, A. P.; Burant, J. C.; Iyengar, S. S.; Tomasi, J.; Cossi, M.; Millam, J. M.; Klene, M; Adamo, C.; Cammi, R.; Ochterski, J. W.; Martin, R. L.; Morokuma, K.; Farkas, O.; Foresman, J. B.; Fox, D. J. *Gaussian 16*; Gaussian, Inc.: Wallingford, CT, 2016.
(124) Raghavachari, K. Perspective on "Density functional thermochemistry. III. The role of exact exchange. *Theor. Chem. Acc.* **2000**, *103*, 361−363.
(125) Lee, C.; Yang, W.; Parr, R. G. Development of the Colle-Salvetti correlation-energy formula into a functional of the electron density. *Phys. Rev. B* **1988**, *37*, 785.
(126) Zhao, Y.; Schultz, N. E.; Truhlar, D. G. Design of density functionals by combining the method of constraint satisfaction with parametrization for thermochemistry, thermochemical kinetics, and noncovalent interactions. *J. Chem. Theory Comput.* **2006**, *2*, 364−382.
(127) Galindo-Murillo, R.; Roe, D. R.; Cheatham, T. E., III Convergence and reproducibility in molecular dynamics simulations of the DNA duplex d (GCACGAACGAACGAACGC). *Biochimica et Biophysica Acta (BBA)-General Subjects* **2015**, *1850*, 1041−1058.
(128) Galindo-Murillo, R.; Roe, D. R.; Cheatham, T. E. On the absence of intrahelical DNA dynamics on the μs to ms timescale. *Nat. Commun.* **2014**, *5*, 5152.
(129) Abdi, H.; Williams, L. J. Principal component analysis. *Wiley interdisciplinary reviews: computational statistics* **2010**, *2*, 433−459.
(130) Fuglebakk, E.; Echave, J.; Reuter, N. Measuring and comparing structural fluctuation patterns in large protein datasets. *Bioinformatics* **2012**, *28*, 2431−2440.
(131) Durrant, J. D.; de Oliveira, C. A. F.; McCammon, J. A. POVME: an algorithm for measuring binding-pocket volumes. *Journal of Molecular Graphics and Modelling* **2011**, *29*, 773−776.
(132) Wagner, J. R.; Sørensen, J.; Hensley, N.; Wong, C.; Zhu, C.; Perison, T.; Amaro, R. E. POVME 3.0: software for mapping binding pocket flexibility. *J. Chem. Theory Comput.* **2017**, *13*, 4584−4592.
(133) Lucet, I. S.; Fantino, E.; Styles, M.; Bamert, R.; Patel, O.; Broughton, S. E.; Walter, M.; Burns, C. J.; Treutlein, H.; Wilks, A. F.; et al. The structural basis of Janus kinase 2 inhibition by a potent and specific pan-Janus kinase inhibitor. *Blood* **2006**, *107*, 176−183.
(134) Williams, N. K.; Bamert, R. S.; Patel, O.; Wang, C.; Walden, P. M.; Wilks, A. F.; Fantino, E.; Rossjohn, J.; Lucet, I. S. Dissecting specificity in the Janus kinases: the structures of JAK-specific inhibitors complexed to the JAK1 and JAK2 protein tyrosine kinase domains. *Journal of molecular biology* **2009**, *387*, 219−232.

https://doi.org/10.1021/acs.jcim.2c01589
J. Chem. Inf. Model. 2023, 63, 2469−2482